Silence of TRIB3 Suppresses Atherosclerosis and Stabilizes Plaques in Diabetic ApoE$^{-/-}$/LDL Receptor$^{-/-}$ Mice

Zhi-hao Wang,[1] Yuan-yuan Shang,[1] Shun Zhang,[2] Ming Zhong,[1] Xu-ping Wang,[1] Jing-ti Deng,[3] Jie Pan,[2] Yun Zhang,[1] and Wei Zhang[1]

Insulin resistance triggers the developments of diabetes mellitus and atherosclerosis. Tribbles homolog 3 (TRIB3) is involved in insulin resistance. We aimed to investigate whether TRIB3 is implicated in diabetic atherosclerosis. Sixty 3-week-old apolipoprotein E (ApoE$^{-/-}$)/LDR receptor (LDLR$^{-/-}$) mice were randomly divided into chow and diabetes groups. Diabetes was induced by a high-fat and high-sugar diet combined with low-dose streptozotocin. Mice in both groups were randomly divided into vehicle and TRIB3-silencing groups. After transfection, all mice were killed to evaluate the effects of TRIB3 on atherosclerosis. Silence of TRIB3 markedly decreased insulin resistance ($P = 0.039$) and glucose ($P = 0.019$), regardless of diabetes. Ultrasonography-measured parameters were similar in both groups, with and without silence of TRIB3. However, silence of TRIB3 decreased the aortic atherosclerotic burden ($P = 1 \times 10^{-13}$). Further study showed that in brachiocephalic lesions, fibrous cap thickness, cap-to-core ratio, collagen content, and the number of smooth muscle cells were significantly increased ($P < 0.01$ for all) by silence of TRIB3, whereas lipid and macrophage contents remained unaltered, with the vulnerability index significantly reduced. Moreover, the numbers of apoptotic cells and macrophages in brachiocephalic lesions were both significantly decreased ($P < 0.01$ for both). Macrophage migration was decreased ($P = 4 \times 10^{-4}$) by knocking down TRIB3, whereas adhesion and phagocytosis were increased ($P < 0.05$ for both). Silence of TRIB3 would diminish atherosclerotic burden and increase the plaque stability in diabetic mice. ***Diabetes*** **61:463–473, 2012**

The increased prevalence of type 2 diabetes mellitus (T2DM) has focused attention on the elevated incidence of diabetic atherosclerosis (1). Insulin resistance (IR) is assumed to trigger the developments of T2DM and atherosclerosis (2).

There is general consensus that inhibition of Akt activity leads to IR. Tribbles homolog 3 (TRIB3), inhibiting Akt, is considered a potential inducer of IR (3). Furthermore, TRIB3 has been demonstrated to be involved in lipid metabolism (4) and in impairment of insulin exocytosis (5).

Despite a debate surrounding the role of TRIB3 in IR (3,6), epidemiological studies recognized that TRIB3 was increased in obese humans with IR (7) and in patients with T2DM (8). Therefore, TRIB3 is an excellent candidate for investigating IR and related clinical disorders. Recently, several studies on the Q84R polymorphism of *TRIB3* have provided initial evidence that individual carriers for 84R exhibit a higher risk for T2DM (9) and cardiovascular diseases (10,11). Our preliminary findings of TRIB3 participating in macrophage apoptosis (12), increased atherosclerosis risk for carriers of the polymorphism (11), and a recent article (13) reporting on the macrophage at the crossroads of IR and atherosclerosis prompted us to focus our efforts on understanding the mechanisms underlying the role of TRIB3 in diabetic atherosclerosis.

To identify whether TRIB3 was implicated in the diabetic atherosclerosis process, we specifically explored the functional effects of silencing TRIB3 in apolipoprotein E (apoE)/LDR receptor (LDLR) double-knockout (DKO) (ApoE$^{-/-}$/LDLR$^{-/-}$) mice with diabetes, which are more susceptible to atherosclerosis than ApoE$^{-/-}$ or LDLR$^{-/-}$ mice. In this study, we observed a significant amelioration of IR coupled with decreased atherosclerotic burden in TRIB3-silenced diabetic mice. Together, these data proved that silencing TRIB3 might be explored as part of the approach to reduce the burden of atherosclerotic diseases in T2DM.

RESEARCH DESIGN AND METHODS

All animal procedures were performed in accordance with the institutional guidelines of Qilu Hospital of Shandong University and were approved by Shandong University Institutional Animal Care and Use Committee. Mice were housed five per cage and allowed access to diet and autoclaved water. A schema of the protocol is provided in Supplementary Fig. S1.

Diabetic model and in vivo experiments

Generation of diabetic model. Three-week-old male apoE/LDLR DKO mice were fed a high-fat diet (HFD; 20% fat, 20% sugar, and 1.25% cholesterol). After 6 weeks, the DKO mice underwent an intraperitoneal glucose tolerance test (IPGTT). Any mouse exhibiting IR was injected once with low-dose streptozotocin (STZ, 75–80 mg/kg i.p.) to induce partial insulin deficiency. Two weeks after the STZ injection, most HFD/STZ-treated mice displayed hyperglycemia, IR, and glucose intolerance, as previously reported (14). At age 11 weeks, animals with similar degrees of hyperglycemia and body weight were randomly divided into vehicle (DM, $n = 15$) and TRIB3-silencing (DM+RNA interference [RNAi], $n = 15$) groups. The mice fed a normal diet were used as nondiabetic controls, divided into chow ($n = 15$) and TRIB3-silenced (chow+RNAi, $n = 15$) groups.

IPGTT. Mice fasted overnight were challenged intraperitoneally with glucose at 1.5 g/kg body weight. Blood glucose levels of every animal were measured from tail blood with the OneTouch SureStep glucometer (LifeScan, Inc., Milpitas, CA) at specified times after glucose administration.

Transfection of recombinant adenovirus full-length *TRIB3* short hairpin RNA was subcloned from pGenesil-1.2 into the pShuttle vector. Then, recombinant pAdxsi adenovirus was constructed using the pAdxsi Adenoviral System

From the [1]Key Laboratory of Cardiovascular Remodeling and Function Research, Chinese Ministry of Education and Chinese Ministry of Public Health; Department of Cardiology, Qilu Hospital of Shandong University, Ji'nan, P.R. China; the [2]Key Laboratory of Animal Resistance Biology of Shandong, College of Life Sciences, Shandong Normal University, Ji'nan, P.R. China; and the [3]Department of Anatomy, Medical School of Shandong University, Ji'nan, P.R. China.

Corresponding author: Wei Zhang, zhangweisdu@gmail.com.

Received 20 April 2011 and accepted 30 September 2011.

DOI: 10.2337/db11-0518

This article contains Supplementary Data online at http://diabetes.diabetesjournals.org/lookup/suppl/doi:10.2337/db11-0518/-/DC1.

Z.-h.W. and Y.-y.S. contributed equally to this work.

See accompanying commentary, p. 265.

(SinoGenoMax, Beijing, P.R. China). After amplification, viruses were purified, titered, and stored at −80°C until used. All mice were administered 5×10^9 plaque-forming units of virus by tail vein injection at 20 weeks and another 5×10^9 plaque-forming units of virus at 22 weeks. The chow group was infected with control virus (vehicle). All mice were killed for further study 2 weeks later.

Serum sampling. At the end of the experiment, the DKO mice were fasted overnight and killed by an overdose of pentobarbital. Fasting serum insulin, glucose, total cholesterol, triglyceride, LDL cholesterol, and HDL cholesterol (HDL-C) were measured. The homeostasis model assessment (HOMA) method was used to calculate IR (15).

Liver glycogen content. Glycogen content was determined by acid hydrolysis and then glucose measurement (16). In brief, 50 mg liver was boiled for 2 h in 0.5 mL of 2 mmol/L HCl and neutralized with an equal volume of 2 mmol/L NaOH. Glucose content was measured using the Glucose (HK) assay kit (Sigma-Aldrich, St. Louis, MO).

Liver triglyceride content. Liver triglycerides were extracted, as previously reported (16), and measured using a Triglyceride Quantification Kit (Abcam, Cambridge, MA), following the manufacturer's instructions for colorimetric assay.

Quantification of atheroma in vivo and in vitro

Ultrasonography. All animals were anesthetized and laid supine on a heated table, and warmed ultrasound transmission gel was placed on the chest. Two-dimensional imaging was performed by using the Real-Time Micro Visualization Scanhead (RMV 704) with a central frequency of 40 MHz at the mechanical transducer (Vevo 770; VisualSonics, Toronto, ON, Canada). Intima-media thickness (IMT) measurements were performed according to previously validated protocols in humans. For each image, three sets of measurements were taken.

Atherosclerotic lesion analysis. Mice were anesthetized and killed. Mouse hearts were perfused with 10 mL phosphate-buffered saline (PBS) and then 10 mL 4% paraformaldehyde (PFA) for 30 min at physiological pressure through the descending aorta. After incubation in 4% PFA overnight, the aorta was cut open longitudinally. To calculate the lesion area, aortas were stained with Oil Red O (Sigma-Aldrich) before the analysis.

Histology. Brachiocephalic arteries were embedded in optimal cutting temperature compound (Sakura Finetek, Beijing, P.R. China). Sections were cut every 30 μm along the brachiocephalic artery and stained with hematoxylin and eosin, Picrosirius red, and Nile red. Quantifications of the lesion areas were performed with Image Pro Plus 5.0 software (Media Cybernetics, Inc., Bethesda, MD).

Immunohistochemistry and transferase-mediated dUTP nick-end labeling staining. For anti-monocyte plus macrophage antibody (MOMA-2) and α-smooth muscle actin staining, frozen sections were fixed with 4% PFA for 20 min before being rinsed with PBS for 15 min at room temperature. Sections were then immersed in 3% H_2O_2, rinsed, and transferred into 5% normal goat serum, followed by staining with rat anti-mouse MOMA-2 antibody (Abcam, Cambridge, U.K.) and horseradish peroxidase-conjugated goat anti-rat secondary antibody. Finally, the sections were developed with DAB (Solarbio, Beijing, China), and some of the sections were counterstained with hematoxylin. Processing of α-smooth muscle actin staining was similar to that for MOMA-2 staining. The staining areas were quantified by Image Pro Plus 5.0.

The vulnerability index was calculated as the ratio of (macrophages + extracellular lipids)/(SM cells + collagen fibers) (17). For transferase-mediated dUTP nick-end labeling (TUNEL) staining, the sections were stained with the In Situ Cell Death Detection Kit-POD or the In Situ Cell Death Detection Kit-TMR Red (Roche, Mannheim, Germany). In brief, sections were immersed in PBS for 15 min at room temperature, incubated in permeabilization solution for 2 min on ice, transferred into the TUNEL reaction mixture, and incubated for 60 min at 37°C in a humidified atmosphere in the dark. Labeling was stopped by transferring sections to PBS. All reagents were provided in the kit, with the exception of PBS.

In vitro experiments

Isolation of peritoneal macrophages. Peritoneal macrophages were harvested from 24-week-old male DKO mice 3 days after an intraperitoneal injection of 40 μg concanavalin A (Sigma-Aldrich) in 0.5 mL sterile PBS. Peritoneal cavities were lavaged twice with 5 mL HyClone Dulbecco's modified Eagle's medium (DMEM; Thermo Fisher Scientific, Waltham, MA), and an aliquot of cells was stained with the MOMA-2 antibody. Generally, 95% of the cells isolated after 72 h were MOMA-2–positive.

Macrophages migration assays. Cell migration assays were performed with 24-well Costar Transwell plates (5 μm). We loaded 75,000 peritoneal macrophages into the upper chambers after overnight starvation. The lower chambers were filled with solution of monocyte chemoattractant protein-1 (100 ng/mL; PeproTech, Inc., Rocky Hill, NJ) in DMEM. After incubation at 37°C for 6 h, macrophages attached to both surfaces of the inserts were fixed and stained with crystal violet (Sigma-Aldrich). Macrophages on the upper side of the membrane were removed by a cotton swab. The average number of macrophages on the lower side was counted.

Adhesion assay. Five million peritoneal macrophages were added into Costar culture plates precoated with 50 μg/mL poly-lysine (Sigma-Aldrich). After incubation at 37°C for 10 min, the adherent cells were stained by DAPI and counted under a fluorescence microscope.

Phagocytosis assay. Peritoneal macrophages were seeded to 12-well plates or glass bottom microwell dishes (MatTek Corporation, Ashland, MA) at a density of 1×10^6 cells/well for 3 h at 37°C. The medium was changed to DMEM containing 10 μg/mL Alexa Fluor 488 AcLDL (Molecular Probes, Invitrogen, Eugene, OR) for 10 min at 37°C. Excessive acetylated LDL was washed away, and the macrophages were detached by trypsinization and analyzed by a flow cytometry (FACSCaliber; BD Biosciences Franklin Lakes, NJ). Those in the glass bottom microwell dishes were fixed and stained by DAPI and observed under a laser scanning confocal microscope (Leica TCS SP2; Leica, Wetzlar, Germany).

***Quantitative real-time PCR for* TRIB3.** Total RNA was isolated from each aorta with the TRIzol reagent (Invitrogen). Total RNA was quantified by spectrophotometry and reverse-transcribed with the M-MLV Reverse Transcriptase System (Promega, Madison, WI) and oligo(dT) primers. The mRNA levels for *TRIB3* were determined by SYBR green (Applied Biosystems) real-time PCR using 10 ng of total RNA, following the manufacturer's instructions. The PCR primers for *TRIB3* were 5′-TCAAGCTGCGTCGCTTTGTC-3′ (forward) and 5′-AGCTGAGTATCTCTG GTCCCACGTA-3′ (reverse); those for β-actin were 5′-CAACTTGATGTATGAAGGCTTTGGT-3′ (forward) and 5′-ACTTTTATTGGTCTCAAGTCAGTGTAC AG-3′ (reverse). All values obtained were normalized to mouse β-actin.

Western blot analysis. Tissues were snap-frozen in liquid nitrogen, pulverized, and resuspended in ice-cold lysis buffer (Solarbio). Protein concentrations were determined with the Bradford method. Lysates were allowed to solubilize on ice for 30 min, and particulate mass was removed by centrifugation (15,000*g*) for 15 min at 4°C. Supernatants were analyzed by SDS-PAGE. Primary antibodies used included TRIB3 polyclonal antibody (p-Ab) (Imgenex, San Diego CA) and Akt p-Ab, phospho-Akt473 p-Ab, cleaved caspase 3 p-Ab, and caspase 3 p-Ab (Cell Signaling Technology, Danvers, MA). Secondary antibodies were horseradish peroxidase-labeled antibodies (Thermo Scientific Pierce, Rockford IL). Blots were processed for enhanced chemifluorescence using a Pierce ECL Western blotting substrate (Thermo Scientific Pierce).

Statistics. All data are presented as mean ± SD and were analyzed by paired and unpaired, two-tailed Students *t* test, one-way ANOVA, and 2 × 2 factorial ANOVA as appropriate. A value of $P < 0.05$ was considered significant. Data were analyzed using SPSS 13.0 software (SPSS Inc., Chicago, IL).

RESULTS

Generation of diabetic atherosclerosis mouse model. To generate a nongenetic rodent model closely resembling human diabetic atherosclerosis disease, HFD alone could induce IR after 6 weeks, confirmed by IPGTT, whereas the combination of HFD and STZ treatment led to frank hyperglycemia and IR (Fig. 1*B*). At the end of the experiment, DM mice still showed significantly elevated blood glucose ($P = 0.026$, Table 1). The mean body weight was significantly higher for DM than normal-chow mice at the age of 9 weeks (Fig. 1*A*).

High-resolution ultrasonography examination revealed atherosclerotic plaques in the arteries of DM mice (Fig. 1*C*), and DM mice showed significantly greater aortic and brachiocephalic IMT than those of chow mice at the age of 20 weeks, with no significant difference at the age of 24 weeks. However, carotid IMT was significantly increased in DM mice at 24 weeks (Fig. 1*D*). The HFD/STZ mouse model showed typical T2DM features of hyperglycemia, IR, and obesity that could persist throughout the experiment. As expected, these DM mice showed significantly more atherosclerosis, as indicated by ultrasonography.

Silence of TRIB3 in aorta. The relative mRNA expression of *TRIB3* in the aorta was significantly increased in DM mice compared with that in chow mice (4.97 ± 1.30 vs. 1.69 ± 0.76, $P = 1 \times 10^{-7}$), whereas silence of TRIB3 significantly reduced relative *TRIB3* mRNA expression in DM (4.97 ± 1.30 vs. 1.59 ± 0.52, $P = 1 \times 10^{-7}$) by 68.01% compared with 35.50% in chow mice (1.69 ± 0.76 vs. 1.09 ± 0.32, $P = 2 \times 10^{-4}$).

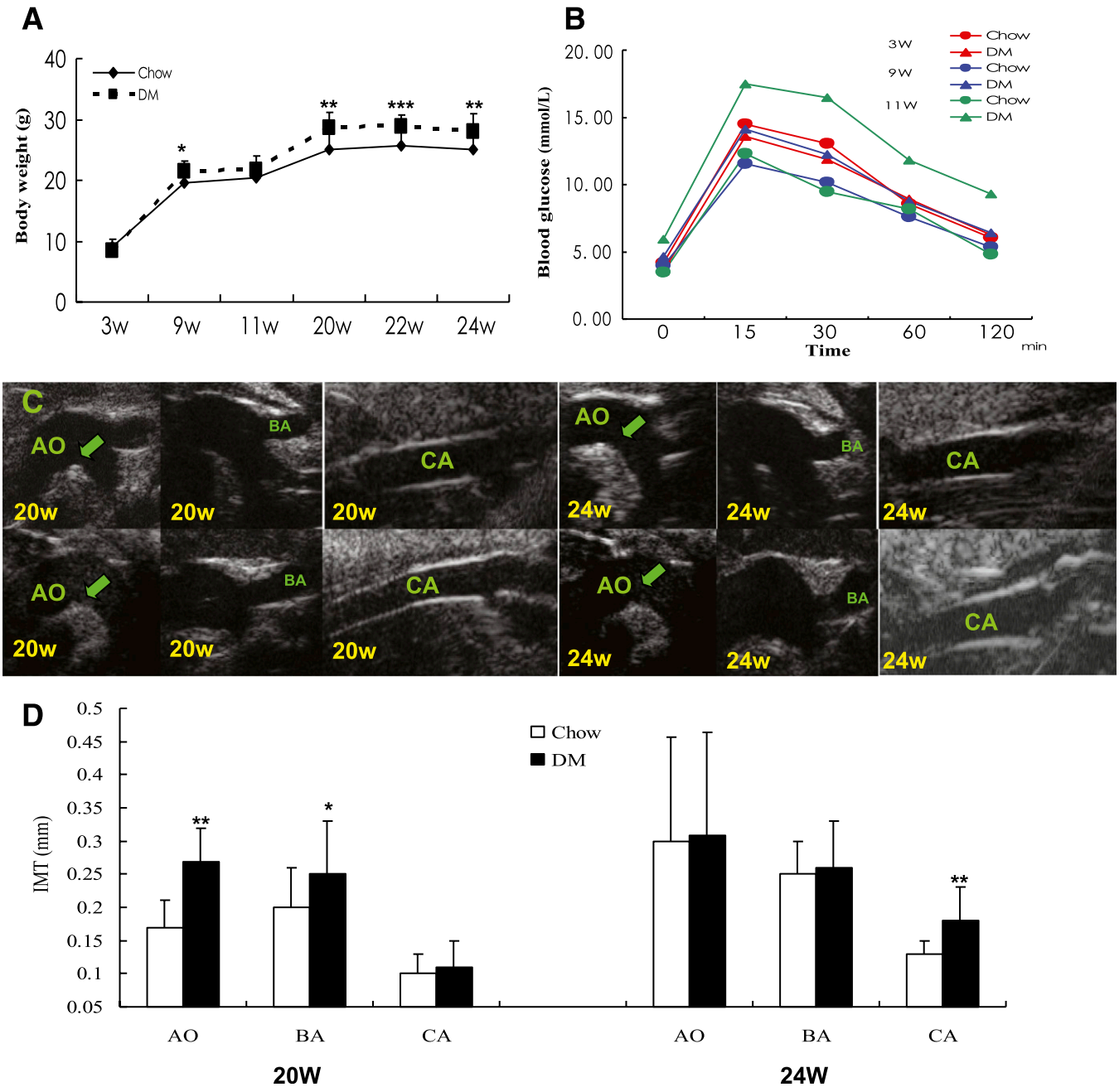

FIG. 1. Generation of diabetic atherosclerosis mouse model. *A*: Body weights of ApoE$^{-/-}$/LDLR$^{-/-}$ mice on a chow diet and an HFD were measured at the ages of 3, 9, 11, 20, 22, and 24 weeks. Unpaired two-tailed Student *t* test was performed. *B*: Glucose response to an intraperitoneal glucose challenge in ApoE$^{-/-}$/LDLR$^{-/-}$ mice at the ages of 3, 9, and 11 weeks. Blood glucose and plasma insulin levels were determined at baseline (after an overnight fast) and at 15, 30, 60, and 120 min after administration of 1.5 g glucose/kg body weight. Paired two-tailed Student *t* test was used (n = 15 mice per group). *C*: Ultrasonography of mouse atherosclerosis, including the aorta (AO), brachiocephalic artery (BA) branch, and the carotid artery (CA) at the ages of 20 and 24 weeks. The images were acquired using a 40-MHz Scanhead (RMV 704). Plaques are indicated by green arrows. *Upper panel* from chow mice and *bottom panel* from DM mice. DM mice had significantly higher aortic (P = 0.001) and brachiocephalic IMT (P = 0.032) than those of chow mice at the age of 20 weeks, but no significant difference was detected at the age of 24 weeks. However, carotid IMT could be found significantly increased at the age of 24 weeks (P = 0.001). *D*: Quantification of atherosclerosis in ApoE$^{-/-}$/LDLR$^{-/-}$ mice by ultrasonography-measured IMT. Unpaired two-tailed Student *t* test was performed. W, week. *P < 0.05, **P < 0.01, ***P < 0.001 vs. chow group. (A high-quality digital representation of this figure is available in the online issue.)

Silence of TRIB3 improves metabolism. Knocking down TRIB3 in this mice model led to a significant decrease in blood glucose in DM mice (P = 0.019, Table 1) and in chow mice (7.00 ± 4.54 vs. 3.80 ± 1.71, P = 0.033, Table 1). However, DM and RNAi silencing of TRIB3 showed no significant interactions (P = 0.375, Table 1). Furthermore, silence of TRIB3 had a similar effect on HOMA-IR (Table 1). Body weight, insulin, cholesterol, and LDL levels were not significantly altered by TRIB3 silence. Further studies showed that liver glycogen content was significantly increased (2.59 ± 0.30 vs. 4.79 ± 0.57, $P = 2 \times 10^{-7}$, Table 1) with silence of TRIB3, but not the hepatic triglyceride level (Table 1).

Silence of TRIB3 decreases aortic atherosclerotic burden. Silencing TRIB3 decreased the number and size of aortic plaques, regardless of diabetes status. Face-to-face

TABLE 1
Metabolic parameters of ApoE$^{-/-}$/LDLR$^{-/-}$ mice

Variable	Chow (n = 15)	DM (n = 15)	Chow+RNAi (n = 15)	DM+RNAi (n = 15)	P*		
					DM	RNAi	Interaction
20 weeks							
Body weight (g)	26.68 ± 2.89	29.50 ± 2.74	25.47 ± 1.61	28.48 ± 1.94	—	—	—
Heart rate (bpm)	622 ± 56	551 ± 114	632 ± 57	580 ± 106	—	—	—
SBP (mmHg)	95.36 ± 14.64	111.33 ± 9.31	83.89 ± 5.93	101.00 ± 6.51	—	—	—
DBP (mmHg)	55.38 ± 6.72	65.83 ± 9.79	48.11 ± 3.18	66.00 ± 6.78	—	—	—
MBP (mmHg)	68.63 ± 8.11	80.83 ± 9.37	59.89 ± 2.93	77.50 ± 5.75	—	—	—
24 weeks							
Body weight (g)	25.10 ± 3.12	28.98 ± 1.95	24.49 ± 1.86	26.20 ± 2.95	0.001	0.112	0.481
Heart rate (bpm)	485 ± 92	583 ± 128	590 ± 91	483 ± 69	0.309	0.520	0.296
SBP (mmHg)	91.63 ± 9.05	104.83 ± 5.60	88.78 ± 13.47	99.50 ± 3.51	0.00004	0.004	0.422
DBP (mmHg)	47.38 ± 12.30	67.67 ± 8.33	53.00 ± 8.94	56.00 ± 8.12	0.000003	0.044	0.671
MBP (mmHg)	62.00 ± 9.67	79.50 ± 6.89	64.78 ± 9.55	70.50 ± 5.82	0.00001	0.028	0.605
Glucose (mmol/L)	7.00 ± 4.54	11.18 ± 10.28	3.80 ± 1.71	4.30 ± 3.27	0.026	0.019	0.375
Insulin (μIU/mL)	19.50 ± 17.78	47.98 ± 43.19	15.39 ± 16.46	42.60 ± 26.59	0.001	0.607	0.686
HOMA-IR	4.45 ± 4.70	16.81 ± 17.96	3.47 ± 5.38	7.42 ± 7.13	0.015	0.039	0.647
Triglycerides (mmol/L)	3.18 ± 3.22	2.81 ± 2.39	4.28 ± 4.16	2.79 ± 1.34	0.303	0.549	0.535
Cholesterol							
Total (mmol/L)	17.07 ± 6.43	21.48 ± 8.60	19.11 ± 8.47	27.40 ± 10.59	0.039	0.187	0.517
LDL (mmol/L)	9.45 ± 3.78	15.17 ± 7.35	12.45 ± 6.88	18.54 ± 7.00	0.010	0.152	0.933
HDL (mmol/L)	3.70 ± 0.95	6.28 ± 2.96	6.07 ± 2.73	8.11 ± 2.68	0.009	0.017	0.748
Liver							
Glycogen (μmoL glu/g tissue)	3.58 ± 1.01	2.59 ± 0.30	6.10 ± 1.41	4.79 ± 0.57	0.002	2×10^{-7}	0.632
Triglycerides (μmoL/g tissue)	20.71 ± 3.21	20.60 ± 2.33	19.31 ± 2.67	21.12 ± 3.61	0.943	0.744	0.408

Data are expressed as mean ± SD. A 2 × 2 factorial ANOVA was used. Serum sampling was taken under fasting condition and measured. bpm, beats per minute; DBP, diastolic blood pressure; MBP, mean blood pressure; SBP, systolic blood pressure; glu, glucose. *P value for DM means comparison of DM with chow. The P value of RNAi means comparison of DM with DM+RNAi.

inspection showed that significantly more areas were covered by atherosclerotic lesions in DM mice than in chow mice (30.99 ± 3.12 vs. 17.00 ± 3.12%, $P = 1 \times 10^{-17}$, Fig. 2*B* and *C*). At 4 weeks after transfection, DM mice showed significantly reduced lesion areas compared with DM+RNAi mice (30.99 ± 3.12 vs. 22.54 ± 2.13%, $P = 1 \times 10^{-13}$, Fig. 2*B* and *C*). Furthermore, chow+RNAi mice demonstrated significantly reduced of atherosclerotic burden compared with chow mice (5.43 ± 1.22 vs. 17.00 ± 3.12%, $P = 4 \times 10^{-14}$, Fig. 2*B* and C).

Silencing TRIB3 stabilized lesions in the brachiocephalic artery. Spontaneous plaque rupture has been demonstrated in the brachiocephalic artery of mice (18). Fibrous cap thickness was significantly reduced in DM mice compared with chow mice ($P = 2 \times 10^{-6}$, Table 2 and Fig. 3, *upper panel*) but was significantly increased in DM+RNAi mice compared with DM mice ($P = 0.021$, Table 2 and Fig. 3, *upper panel*), with no change in chow mice. Further factorial analyses showed significant interactions between DM and RNAi for fibrous cap thickness ($P = 1 \times 10^{-9}$, Table 2 and Fig. 3, *upper panel*), suggesting the benefit of silencing TRIB3 in DM. Because silence of TRIB3 would improve metabolism, even after adjusting for blood pressure, glucose, and HDL-C, it would significantly increase the cap thickness in DM mice ($P = 0.021$, Table 2).

In the current study, the cap-to-core ratio was significantly lower in DM mice than in chow mice ($P = 0.033$), while silencing TRIB3 significantly increased the ratio in DM ($P = 0.025$) and chow mice ($P = 0.043$). Further factorial analyses showed no significant interactions between DM and RNAi ($P = 0.625$), indicating that silenced TRIB3 and DM independently exerted effects on the ratio. However, after adjusting for blood pressure, glucose, and HDL-C, silence of TRIB3 had no effect on the ratio ($P = 0.914$, Table 2).

After adjusting for blood pressure, glucose, and HDL-C, collagen content was significantly lower in DM mice than in chow mice ($P = 0.004$, Table 2 and Fig. 3, *middle panel*), whereas it was significantly increased in DM+RNAi mice compared with DM mice ($P = 0.02$, Table 2 and Fig. 3, *middle panel*), with no difference in chow mice. Subsequent factorial analyses showed significant interactions between DM and RNAi ($P = 0.013$, Fig. 3, *middle panel*). After adjusting for blood pressure, glucose, and HDL-C, no significant interactions between DM and RNAi were revealed ($P = 0.215$, Table 2). Further studies demonstrated that silencing TRIB3 could significantly augment the collagen I-to-III ratio in DM ($P = 0.034$) and chow mice ($P = 0.038$, Fig. 3, *middle panel*), for an increased proportion of collagen I to stabilize the plaques. However, after adjusting for blood pressure, glucose, and HDL-C, silence of TRIB3 had no effect on the collagen I-to- III ratio (Table 2).

Lipid, the other extracellular component, was significantly enhanced in DM mice compared with chow mice ($P = 0.032$, Table 2 and Fig. 3, *bottom panel*) after adjusting for blood pressure, glucose, and HDL-C, and not substantially altered by silencing TRIB3.

The cellular component, smooth muscle cells, was not significantly altered by DM but was significantly increased with TRIB3 silencing. However, macrophage content was significantly higher in DM mice than in chow mice ($P = 0.0005$, Table 2 and Fig. 3, *bottom panel*) after adjusting for blood pressure, glucose, and HDL-C, and not significantly altered by silence of TRIB3.

The vulnerability index, describing the plaque stability, was significantly higher in DM mice than in chow mice

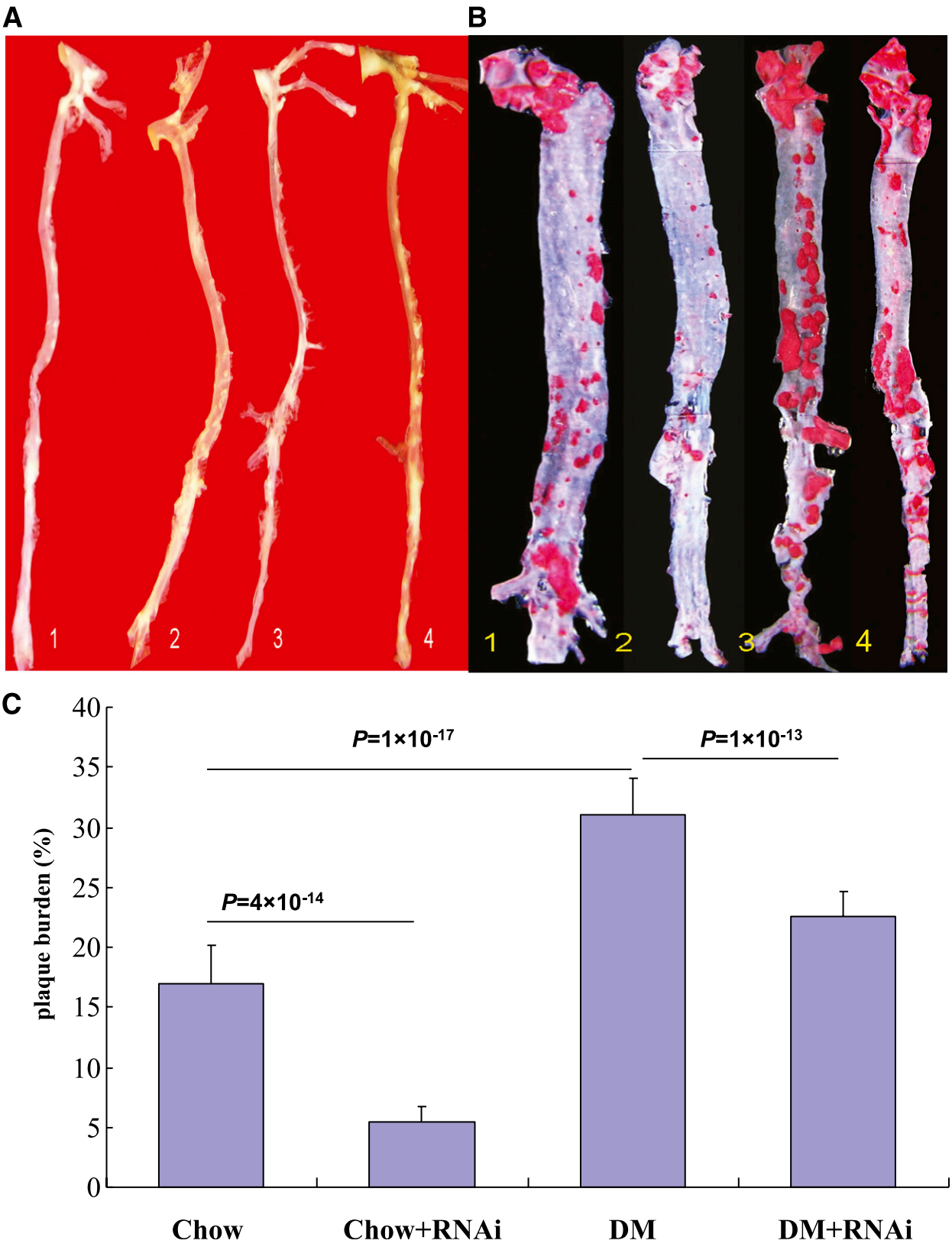

FIG. 2. Images and quantifications of aortic atherosclerotic lesions in ApoE$^{-/-}$/LDLR$^{-/-}$ mice with and without TRIB3 silencing. *A*: Images of aortic atherosclerotic lesions from mice. Experimental groups are indicated as follows: *1*, chow diet (Chow); *2*, chow diet with silence of TRIB3 (chow +RNAi); *3*, DM; *4*, DM with silence of TRIB3 (DM+RNAi). *B*: The degree of atherosclerosis determined by Oil Red O staining of face-to-face lesion areas in ApoE$^{-/-}$/LDLR$^{-/-}$ mice. *C*: Quantification of atherosclerotic lesion areas. One-way ANOVA was performed. (A high-quality digital representation of this figure is available in the online issue.)

TABLE 2
Histology analyses of brachiocephalic atherosclerotic plaques

Variable	Chow (n = 15)	DM (n = 15)	Chow+RNAi (n = 15)	DM+RNAi (n = 15)	P*		
					DM	RNAi	Interaction
Plaque area (mm^2)	0.10 ± 0.06	0.13 ± 0.09	0.07 ± 0.07	0.12 ± 0.08	0.424	0.466	2×10^{-4}
Fibrous cap (μm)	11.28 ± 0.99	4.18 ± 0.60	10.01 ± 1.32	14.52 ± 2.27	2×10^{-6}	0.021	1×10^{-9}
Cap-to-core ratio	0.18 ± 0.07	0.04 ± 0.01	0.30 ± 0.12	0.21 ± 0.13	0.150	0.914	0.034
Collagen content (%)	17.57 ± 1.25	13.07 ± 2.64	17.85 ± 1.54	16.89 ± 2.91	0.004	0.02	0.215
I-to-III collagen ratio	1.71 ± 1.12	1.62 ± 0.67	3.13 ± 1.74	2.85 ± 1.50	0.065	0.738	0.318
Lipid (%)	40.83 ± 8.87	48.63 ± 5.50	42.15 ± 8.42	51.04 ± 14.30	0.032	0.471	0.946
SMC (%)	15.26 ± 4.35	14.86 ± 3.16	19.79 ± 7.68	20.19 ± 5.75	0.393	0.019	0.552
Macrophage (%)	15.61 ± 2.80	32.95 ± 8.56	15.83 ± 4.12	33.06 ± 11.62	0.0005	0.486	0.886
Vulnerability index	1.75 ± 0.45	2.97 ± 0.57	1.59 ± 0.40	2.32 ± 0.59	0.004	0.015	0.245

Data are expressed as mean ± SD. A 2 × 2 factorial ANOVA was used adjusting for blood pressure, glucose, and HDL-C. P was adjusted for blood pressure, glucose, and HDL-C. Fibrous cap was measured at the thinnest part of each plaque (24). SMC, smooth muscle cell. *The P value for DM means comparison of DM with chow. The P value of RNAi means comparison of DM with DM+RNAi.

(P = 0.004, Table 2) after adjusting for blood pressure, glucose, and HDL-C, whereas silence of TRIB3 significantly decreased the vulnerability index in DM (P = 0.015, Table 2) but not chow mice. Further factorial analyses showed no significant interactions between DM and RNAi for the vulnerability index (P = 0.245, Table 2), indicating that silencing TRIB3 and DM independently exert effects on the vulnerability index. Even with no adjustment for blood pressure, glucose, and HDL-C, silence of TRIB3 significantly decreased the vulnerability index (Table 2).

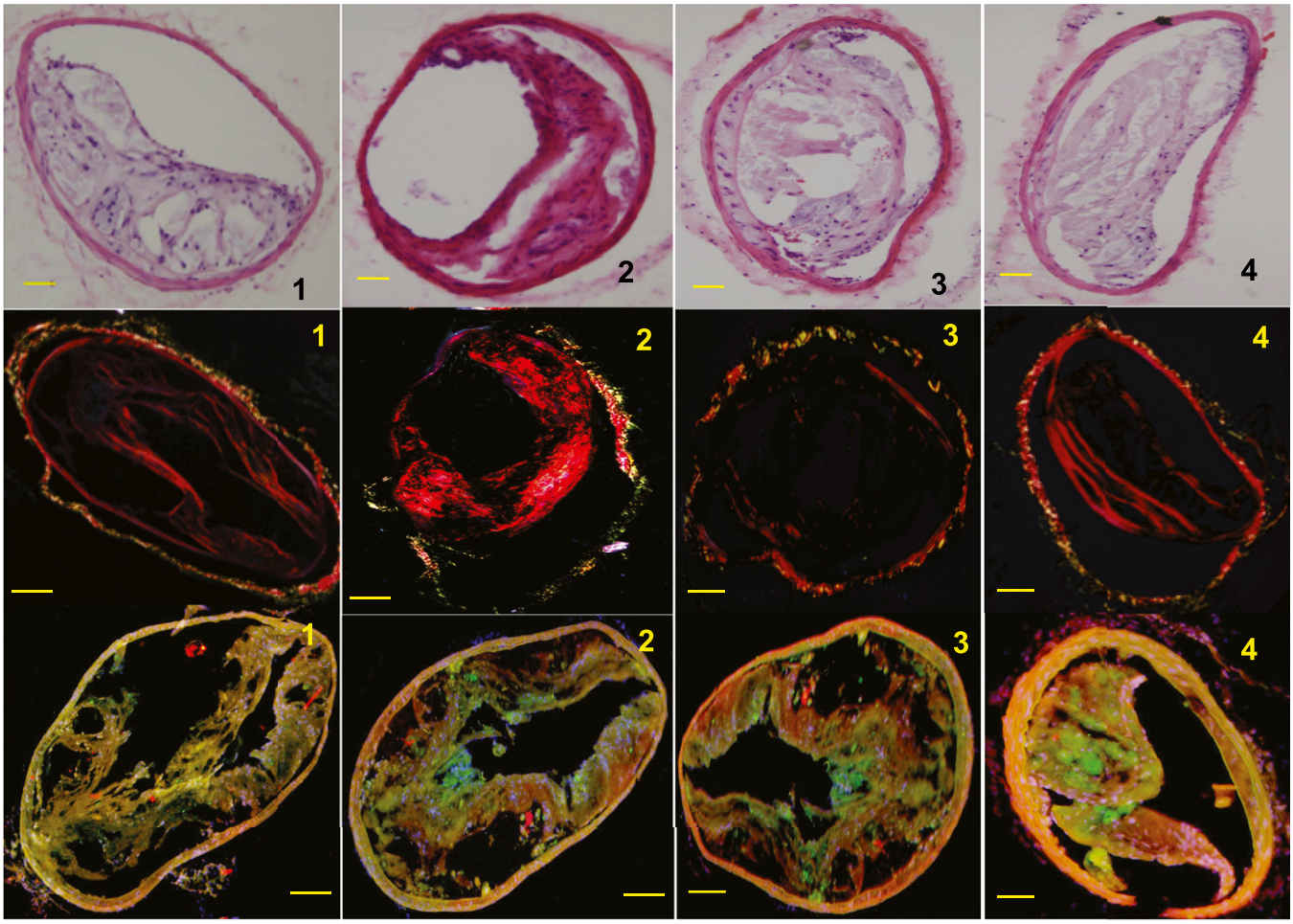

FIG. 3. Histological analyses of brachiocephalic artery lesions of ApoE$^{-/-}$/LDLR$^{-/-}$ mice with and without TRIB3 silencing. *Top panel* shows sample cross-sections of brachiocephalic artery stained with hematoxylin and eosin. *Middle panel* shows atherosclerotic lesions in brachiocephalic artery stained with Picrosirius red for collagen. *Bottom panel* shows atherosclerotic lesions in brachiocephalic artery stained with the microphage marker MOMA-2 (green), lipid marker Nile red (yellow), and nuclei marker DAPI (blue). Experimental groups are indicated as follows: *1*, chow diet (Chow); *2*, chow diet with silence of TRIB3 (Chow+RNAi); *3*, DM; *4*, DM with silence of TRIB3 (DM+RNAi). Scale bar, 100 μm. (A high-quality digital representation of this figure is available in the online issue.)

Silence of TRIB3 decreases macrophage apoptosis in the brachiocephalic artery. Cell apoptosis was significantly greater in DM mice than in chow mice (201.00 ± 61.01 vs. 85.63 ± 38.46, P = 0.00003, Fig. 4), whereas silence of TRIB3 significantly reduced cell apoptosis in DM+RNAi mice compared with DM mice (201.00 ± 61.01 vs. 95.86 ± 39.80, P = 0.0001, Fig. 4), with no effect on chow mice. Further factorial analyses showed significant interactions between DM and RNAi for apoptosis (P = 0.007, Fig. 4).

To evaluate the role of macrophages in plaque stability, macrophage apoptosis was analyzed. We found a significantly higher number of TUNEL-positive, MOMA-2–positive macrophages in lesions from DM mice than in chow mice (108.80 ± 33.44 vs. 48.31 ± 28.39, P = 0.0001, Fig. 4). Silence of TRIB3 significantly decreased macrophage apoptosis in lesions from DM+RNAi mice compared with DM mice (46.20 ± 15.21 vs. 108.80 ± 33.44, P = 0.00006, Fig. 4), with no affect on chow mice. Further factorial analyses showed

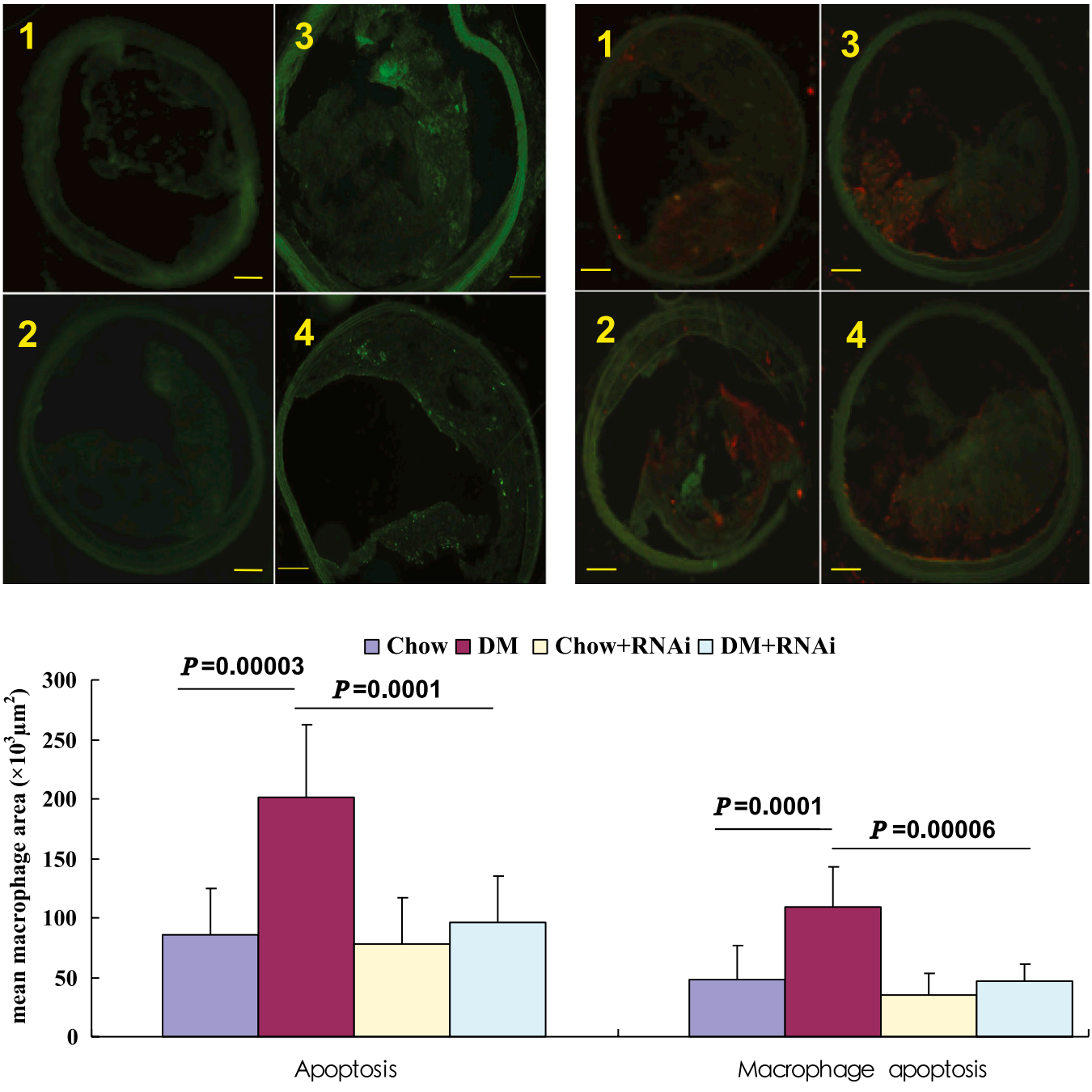

FIG. 4. Apoptotic cell deposition and apoptotic macrophage accumulation in atherosclerotic lesions from brachiocephalic arteries of ApoE$^{-/-}$/LDLR$^{-/-}$ mice. *Top left panel*, apoptotic cells were detected by TUNEL staining (green) in atherosclerotic lesions on brachiocephalic sections of ApoE$^{-/-}$/LDLR$^{-/-}$ mice. *Top right panel*, atherosclerotic lesions were stained with the monocyte/macrophage marker MOMA-2 for visualization of macrophages (green) and TUNEL staining for apoptotic cells (red). *Bottom panel* shows quantification of apoptotic cell deposition and apoptotic macrophage accumulation in atherosclerotic lesions. Experimental groups are indicated as follows: *1*, chow diet (Chow); *2*, chow diet with silence of TRIB3 (Chow+RNAi); *3*, DM; *4*, DM with silence of TRIB3 (DM+RNAi). Scale bar, 100 μm. (A high-quality digital representation of this figure is available in the online issue.)

significant interactions between DM and RNAi for macrophage apoptosis (P = 0.013, Fig. 4), indicating a benefit of silencing TRIB3 in DM.

Knocking down TRIB3 increased Akt activity. The TRIB3 level was higher in DM mice than in chow mice (Fig. 5, *lane 4* vs. *lane 2*). Correspondingly, phosphorylation of Akt was lower (Fig. 5, *lane 4* vs. *lane 2*) in DM mice, and as a consequence, caspase-3 was upregulated in DM mice. However, silencing TRIB3 increased the phosphorylation of Akt in DM+RNAi mice (Fig. 5, *lane 3* vs. *lane 4*). Meanwhile, downregulation of caspase-3 was detected in DM+RNAi mice. These phenomena were also observed in chow mice.

Silence of TRIB3 and macrophage functions. To test whether TRIB3 silence exerted an effect on macrophage adhesion, migration, and phagocytosis, peritoneal macrophages isolated from four different groups were examined. We first examined the effects of TRIB3 deficiency on chemotaxis by Transwell migration assay. DM mice showed significantly more migrated macrophages than did chow mice (14.00 ± 2.45 vs. 5.60 ± 2.37, $P = 1 \times 10^{-8}$, Fig. 6*A* and *E*). Silence of TRIB3 significantly decreased macrophage migration from DM+RNAi mice compared with DM mice (7.10 ± 3.28 vs. 14.00 ± 2.45, $P = 4 \times 10^{-4}$, Fig. 6*A* and *E*). Migration of macrophages was equivalent in cells isolated from both groups of chow mice (P = 0.603, Fig. 6*A* and *E*). Further factorial analyses showed significant interactions between DM and RNAi for macrophage migration ($P = 4 \times 10^{-4}$, Fig. 6*E*), indicating benefit of silencing TRIB3 in DM.

Peritoneal macrophages from DM mice showed significantly increased macrophage adherence to the surfaces coated with poly-lysine compared with those from chow mice (44.83 ± 8.81 vs. 25.71 ± 2.50%, $P = 3 \times 10^{-4}$, Fig. 6*B* and *F*). Silence of TRIB3 significantly increased macrophage adhesion from chow+RNAi mice compared with chow mice (34.07 ± 9.00 vs. 25.71 ± 2.50%, P = 0.020, Fig. 6*B* and *F*), with no effect on DM mice (P = 0.515, Fig. 6*B* and *F*). Further factorial analyses showed no significant interactions between DM and RNAi for macrophage adhesion (P = 0.142), which suggests that silencing TRIB3 and DM independently exert effects on macrophage adhesion.

Flow cytometry analysis revealed significantly higher phagocytosis ability of macrophages for DM mice than for chow mice (47.50 ± 15.92 vs. 27.67 ± 0.77, P = 0.004, Fig. 6*G*, *C*, and *D*). Silence of TRIB3 significantly increased macrophage phagocytosis, regardless of DM (Fig. 6*G*, *C*, and *D*). Further factorial analyses showed no significant interactions between DM and RNAi for macrophage phagocytosis (P = 0.131), which suggests that silencing TRIB3 and DM independently exert effects on macrophage phagocytosis.

DISCUSSION

Because IR triggers the development of DM and atherosclerosis and TRIB3 is involved in IR, we aimed to investigate whether TRIB3 is implicated in diabetic atherosclerosis in mice. We found that silence of TRIB3 in vivo improved metabolism, alleviated the atherosclerotic lesion burden, and stabilized atherosclerotic plaque in a mouse model of diabetic atherosclerosis. Mechanistically, this phenotype is attributed to a decrease in proatherogenic pathways, such as increased Akt phosphorylation, amelioration of IR, and diminished macrophage apoptosis. To our knowledge, these findings provide novel insights into the molecular

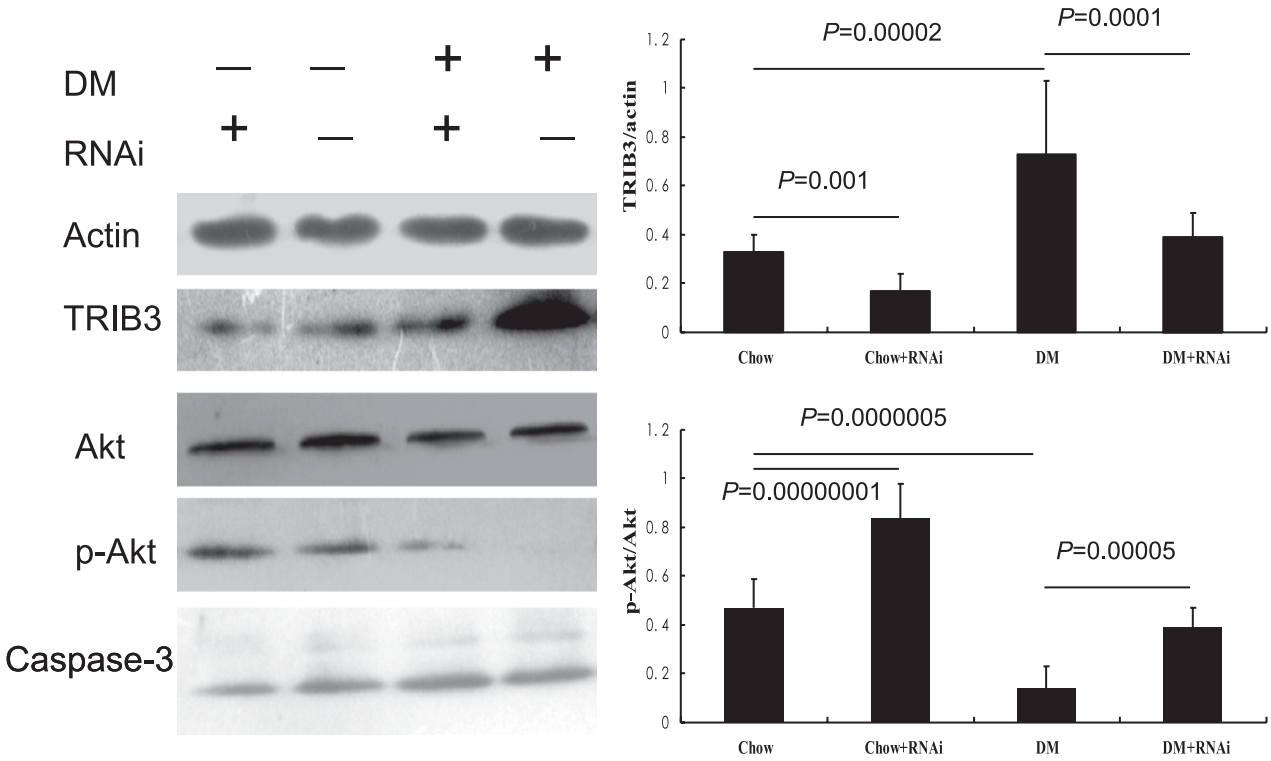

FIG. 5. Western blot analyses of TRIB3, Akt, phospho-Akt573 (p-Akt), and activated caspase-3 in aorta from ApoE$^{-/-}$/LDLR$^{-/-}$ mice (n = 5 mice per group). The Western blots are representative of two separate experiments that gave similar results. One-way ANOVA was performed.

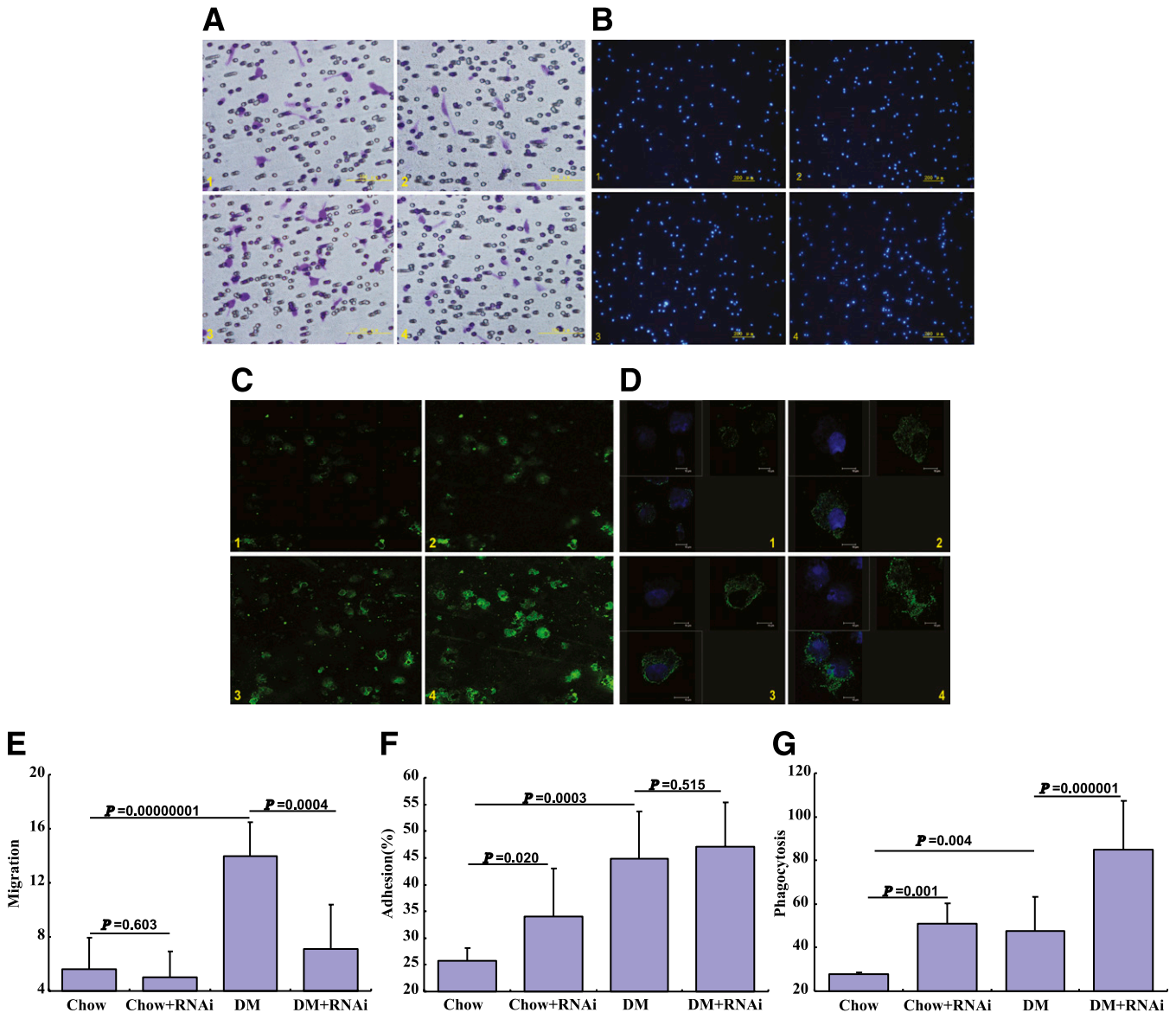

FIG. 6. Effects of silence of TRIB3 on peritoneal macrophage functions. Images and quantification of peritoneal macrophage migration (*A* and *E*), adhesion (*B* and *F*), and phagocytosis (*C*, *D*, and *G*). *A*: Peritoneal macrophages were added to the top chambers of Transwell plates. Monocyte chemoattractant protein-1 (100 ng/mL) was added to the lower chambers. After a 6-h incubation, cells attached to both surfaces of inserts were fixed and stained with crystal violet (Sigma-Aldrich), and those on the upper side of the membrane were removed with a cotton swab. The macrophages on the lower side were counted and analyzed. *E*: Quantification of peritoneal macrophage migration. *B*: Peritoneal macrophages were added onto 24-well plates coated with poly-lysine. After 10 min, attached cells were fixed, stained by DAPI, and counted. *F*: Quantification of peritoneal macrophage adhesion. Peritoneal macrophages were seeded to glass bottom microwell dishes. Alexa Fluor 488 AcLDL was added to the cells for 10 min. After extensive washes, cells were fixed and observed under a fluorescence microscope (*C*) or laser scanning confocal microscope (*D*). *G*: Peritoneal macrophages were seeded to 12-well plates. Alexa Fluor 488 AcLDL was added to the cells for 10 min. After extensive washes, cells were detached and analyzed by fluorescence-activated cell sorter. Experimental groups are indicated as follows: *1*, chow diet (Chow); *2*, chow diet with silence of TRIB3 (Chow+RNAi); *3*, DM; *4*, DM with silence of TRIB3 group (DM+RNAi). One-way ANOVA was performed. (A high-quality digital representation of this figure is available in the online issue.)

mechanisms that directly link TRIB3 to atherosclerosis in DM.

Amelioration of DM metabolisms with TRIB3 silencing. TRIB3 was found to inhibit insulin-stimulated Akt phosphorylation (3) and modulate gluconeogenesis in rodent liver (19). Several studies demonstrated TRIB3 induction as a novel molecular mechanism in human IR and diabetes (5,7,8). Previous research has described that a gain-of-function mutation of TRIB3 is associated with IR and related abnormalities (9–11). In the current study, TRIB3 expression was higher in the mouse models of diabetes. Moreover, silence of TRIB3 could ameliorate IR and lower blood glucose, which might be attributed to increased phosphorylation of Akt, crucial for insulin signaling (3).

Silence of TRIB3 decreases atherosclerotic burden. TRIB3 has been revealed to be upregulated in atherosclerotic unstable plaque (20). Studies demonstrated that TRIB3 is upregulated by oxidized LDL (21) and mediates human monocyte-derived macrophage apoptosis (22). However, the impact of silence of TRIB3 on plaque progression remained to be specifically investigated. Here, we detected upregulated TRIB3 in the diabetic atherosclerotic mice, which was accompanied by increased macrophage apoptosis in the

atherosclerotic plaque. With the silence of TRIB3, the aortic atherosclerotic burden and lesion formation were mitigated. Furthermore, data from nondiabetic mice showed the atherosclerotic burden was reduced by silence of TRIB3 even if IR was not significantly improved.

Stabilization of atherosclerotic plaque by knocking down TRIB3. Some phenotypic characteristics of atherosclerotic plaques, such as fibrous cap thickness, collagen content, plaque cap-to-core ratio, and macrophage number have been widely used as indicators of plaque stability. We confirmed that DM mice had thinner fibrous caps than chow mice and that silencing TRIB3 could lead to thicker fibrous caps. The fibrous cap consists of collagen, and we found that the collagen content of plaques was lower in DM mice than in chow mice, whereas silence of TRIB3 increased the collagen content of plaques to stabilize it.

Plaques with a thin fibrous cap and a large lipid core are considered vulnerable (23). Hence, we analyzed the cap-to-core ratio to determine the plaque vulnerability. The ratio was lower in DM mice than in chow mice, and silence of TRIB3 enhanced the ratio to stabilize the plaque. However, silence of TRIB3 had no effect on the ratio when controlling for the metabolic factors, which suggests that the ratio might depend more on metabolism. Investigation of the vulnerability index demonstrated that silence of TRIB3 increased the stability of plaque when controlling for the metabolic factors.

Macrophages with silence of TRIB3. The macrophages were thought to be at the crossroad of IR and atherosclerosis (13). IR in macrophages, more susceptible to apoptosis, may promote the development of atherosclerosis, thus increasing the vulnerability. Therefore, silence of TRIB3 should ameliorate IR and thereby reduce macrophage apoptosis in diabetic atherosclerosis in vivo, in agreement with our findings in vitro (12).

Further study showed that macrophages from DM mice exhibited increased migration, enhanced adherence, and augmented phagocytosis, which were altered by silence of TRIB3. Increased migration suggested enhanced macrophage recruitment, which has important roles in atherogenesis. Knocking down TRIB3 would significantly decrease macrophage migration to prohibit atherosclerotic plaque expansion. Enhanced adherence indicates an increased ability of tissue infiltration under diabetic conditions. Knocking down TRIB3 increased the adhesion only in chow mice, whereas this function maintained unchanged in DM mice, which might be attributable to increased local clearance. Phagocytosis was amplified by silence of TRIB3 in both mouse types, which indicates that more necrotic lipid was engulfed by macrophages. Therefore, augmented phagocytosis with silence of TRIB3 suggested regained phagocytic clearance, which would restrain expansion of the necrotic core.

Limitation. Adenoviral gene delivery by tail vein injection is a simple yet effective in vivo gene-delivery method. Because of tail vein injection, the observed effect in macrophages could be derived from a direct action of TRIB3 small interfering RNA in those macrophages and an indirect effect of TRIB3 mRNA knockdown on whole-body insulin sensitivity mice in the current study. Because intravenous delivery is minimally invasive and easily manipulated, it is increasingly being used to elucidate the role of genes in the pathogenesis of disease in animal models.

In conclusion, we collectively found that silence of TRIB3 diminishes the atherosclerotic burden and increases plaque stability in diabetic atherosclerotic mice, which might provide a therapeutic approach to decreasing atheroma formation and promoting plaque stabilization in diabetes state.

ACKNOWLEDGMENTS

This work was supported by research grants from the Key Technologies R & D Program of Shandong Province (2006GG2202020 and 2010G0020262), the Natural Science Foundation of Shandong Province (Y2005C11, ZR2009CM022, ZR2009CM025, and BS2009YY026), the National Natural Science Foundation of China (30670874, 30871038, 30971215, 81070192, 81070141, and 81100605), and the National Basic Research Program of China (973 Program, Grant No.: 2009CB521904).

No potential conflicts of interest relevant to this article were reported.

Z.-h.W. wrote the manuscript and researched data. Y.-y.S. and S.Z. researched data. M.Z., J.-t.D., and J.P. reviewed and edited the manuscript. X.-p.W. contributed to discussion and reviewed and edited the manuscript. Y.Z. researched data and contributed to discussion. W.Z. wrote the manuscript.

REFERENCES

1. Milicevic Z, Raz I, Beattie SD, et al. Natural history of cardiovascular disease in patients with diabetes: role of hyperglycemia. Diabetes Care 2008;31(Suppl. 2):S155–S160
2. Van Gaal LF, Mertens IL, De Block CE. Mechanisms linking obesity with cardiovascular disease. Nature 2006;444:875–880
3. Du K, Herzig S, Kulkarni RN, Montminy M. TRB3: a tribbles homolog that inhibits Akt/PKB activation by insulin in liver. Science 2003;300:1574–1577
4. Qi L, Heredia JE, Altarejos JY, et al. TRB3 links the E3 ubiquitin ligase COP1 to lipid metabolism. Science 2006;312:1763–1766
5. Liew CW, Bochenski J, Kawamori D, et al. The pseudokinase tribbles homolog 3 interacts with ATF4 to negatively regulate insulin exocytosis in human and mouse beta cells. J Clin Invest 2010;120:2876–2888
6. Okamoto H, Latres E, Liu R, et al. Genetic deletion of Trb3, the mammalian Drosophila tribbles homolog, displays normal hepatic insulin signaling and glucose homeostasis. Diabetes 2007;56:1350–1356
7. Oberkofler H, Pfeifenberger A, Soyal S, et al. Aberrant hepatic TRIB3 gene expression in insulin-resistant obese humans. Diabetologia 2010;53:1971–1975
8. Liu J, Wu X, Franklin JL, et al. Mammalian Tribbles homolog 3 impairs insulin action in skeletal muscle: role in glucose-induced insulin resistance. Am J Physiol Endocrinol Metab 2010;298:E565–E576
9. Prudente S, Scarpelli D, Chandalia M, et al. The TRIB3 Q84R polymorphism and risk of early-onset type 2 diabetes. J Clin Endocrinol Metab 2009;94:190–196
10. Prudente S, Hribal ML, Flex E, et al. The functional Q84R polymorphism of mammalian Tribbles homolog TRB3 is associated with insulin resistance and related cardiovascular risk in Caucasians from Italy. Diabetes 2005;54:2807–2811
11. Gong HP, Wang ZH, Jiang H, et al. TRIB3 functional Q84R polymorphism is a risk factor for metabolic syndrome and carotid atherosclerosis. Diabetes Care 2009;32:1311–1313
12. Shang YY, Wang ZH, Zhang LP, et al. TRB3, upregulated by ox-LDL, mediates human monocyte-derived macrophage apoptosis. FEBS J 2009;276:2752–2761
13. Liang CP, Han S, Senokuchi T, Tall AR. The macrophage at the crossroads of insulin resistance and atherosclerosis. Circ Res 2007;100:1546–1555
14. Mu J, Woods J, Zhou YP, et al. Chronic inhibition of dipeptidyl peptidase-4 with a sitagliptin analog preserves pancreatic beta-cell mass and function in a rodent model of type 2 diabetes. Diabetes 2006;55:1695–1704
15. Matthews DR, Hosker JP, Rudenski AS, Naylor BA, Treacher DF, Turner RC. Homeostasis model assessment: insulin resistance and beta-cell function from fasting plasma glucose and insulin concentrations in man. Diabetologia 1985;28:412–419
16. Marsili A, Aguayo-Mazzucato C, Chen T, et al. Mice with a targeted deletion of the type 2 deiodinase are insulin resistant and susceptible to diet induced obesity. PLoS ONE 2011;6:e20832

17. Shiomi M, Ito T, Hirouchi Y, Enomoto M. Fibromuscular cap composition is important for the stability of established atherosclerotic plaques in mature WHHL rabbits treated with statins. Atherosclerosis 2001;157:75–84
18. Johnson JL, Jackson CL. Atherosclerotic plaque rupture in the apolipoprotein E knockout mouse. Atherosclerosis 2001;154:399–406
19. Yao XH, Nyomba BL. Hepatic insulin resistance induced by prenatal alcohol exposure is associated with reduced PTEN and TRB3 acetylation in adult rat offspring. Am J Physiol Regul Integr Comp Physiol 2008;294: R1797–R1806
20. Deng J, James CH, Patel L, et al. Human tribbles homologue 2 is expressed in unstable regions of carotid plaques and regulates macrophage IL-10 in vitro. Clin Sci (Lond) 2009;116:241–248
21. Shang YY, Zhong M, Zhang LP, et al. Tribble 3, a novel oxidized low-density lipoprotein-inducible gene, is induced via the activating transcription factor 4-C/EBP homologous protein pathway. Clin Exp Pharmacol Physiol 2010;37:51–55
22. Gautier EL, Huby T, Witztum JL, et al. Macrophage apoptosis exerts divergent effects on atherogenesis as a function of lesion stage. Circulation 2009;119:1795–1804
23. Rekhter MD. How to evaluate plaque vulnerability in animal models of atherosclerosis? Cardiovasc Res 2002;54:36–41
24. Kume T, Akasaka T, Kawamoto T, et al. Measurement of the thickness of the fibrous cap by optical coherence tomography . Am Heart J 2006;152: 755.e1–755.e4.